

Very Low-Mass Stellar and Substellar Companions to Solar-like Stars From MARVELS VI: A Giant Planet and a Brown Dwarf Candidate in a Close Binary System HD 87646

Bo Ma(馬波)¹, Jian Ge¹, Alex Wolszczan², Matthew W. Muterspaugh^{3,4}, Brian Lee¹, Gregory W. Henry⁴, Donald P. Schneider^{2,6}, Eduardo L. Martín⁷, Andrzej Niedzielski⁸, Jiwei Xie^{1,9}, Scott W. Fleming^{14,15}, Neil Thomas¹, Michael Williamson^{3,4}, Zhaohuan Zhu²⁶, Eric Agol²⁵, Dmitry Bizyaev¹⁰, Luiz Nicolaci da Costa^{11,12}, Peng Jiang^{1,16}, A.F. Martinez Fiorenzano²⁴, Jonay I. González Hernández^{22,23}, Pengcheng Guo¹, Nolan Grieves¹, Rui Li¹, Jane Liu¹, Suvrath Mahadevan^{2,6}, Tsevi Mazeh¹⁷, Duy Cuong Nguyen¹⁸, Martin Paegert⁵, Sirinrat Sithajan¹, Keivan Stassun⁵, Sivarani Thirupathi¹, Julian C. van Eyken¹³, Xiaoke Wan¹, Ji Wang¹⁹, John P. Wisniewski²¹, Bo Zhao¹, Shay Zucker²⁰

boma@astro.ufl.edu

¹Department of Astronomy, University of Florida, 211 Bryant Space Science Center, Gainesville, FL, 32611-2055, USA

²Department of Astronomy and Astrophysics, The Pennsylvania State University, University Park, PA 16802, USA

³Department of Mathematical Sciences, College of Life and Physical Sciences, Tennessee State University, Boswell Science Hall, Nashville, TN 37209, USA

⁴Center of Excellence in Information Systems Engineering and Management, Tennessee State University, 3500 John A. Merritt Blvd., Box No. 9501, Nashville, TN 37209-1561, USA

⁵Department of Physics & Astronomy, Vanderbilt University, Nashville, TN 37235 USA

⁶Center for Exoplanets and Habitable Worlds, The Pennsylvania State University, University Park, PA 16802, USA

⁷Centro de Astrobiología (INTA-CSIC), Carretera de Ajalvir km 4, E-28550 Torrejón de Ardoz, Madrid, Spain

⁸Toruń Centre for Astronomy, Nicolaus Copernicus University in Toruń, Grudziadzka 5, 87-100 Toruń, Poland

⁹Department of Astronomy & Key Laboratory of Modern Astronomy and Astrophysics in Ministry of Education, Nanjing University, Nanjing 210093, China

¹⁰Apache Point Observatory and New Mexico State University, P.O. Box 59, Sunspot, NM, 88349-0059, USA

¹¹Laboratório Interinstitucional de e-Astronomia (LIneA), Rio de Janeiro, RJ, 20921-400, Brazil

¹²Observatório Nacional, Rua General José Cristino, 77, 20921-400 São Cristóvão, Rio de Janeiro, RJ, Brazil

¹³Department of Physics, UC Santa Barbara, Santa Barbara, CA 93106-9530, USA

¹⁴Space Telescope Science Institute, 3700 San Martin Dr., Baltimore, MD, USA 21218

¹⁵Computer Sciences Corporation, 3700 San Martin Dr., Baltimore, MD, USA 21218

¹⁶Key Laboratory for Research in Galaxies and Cosmology, The University of Science and Technology of China, Hefei, Anhui 230026, China

¹⁷School of Physics and Astronomy, Raymond and Beverly Sackler Faculty of Exact Sciences, Tel Aviv University, Tel Aviv 69978, Israel

¹⁸Dunlap Institute for Astronomy and Astrophysics, University of Toronto, Toronto, ON, M5S 3H4, Canada

¹⁹Department of Astronomy, Yale University, New Haven, CT 06511, USA

²⁰Department of Geosciences, Raymond and Beverly Sackler Faculty of Exact Sciences, Tel Aviv University, 6997801 Tel Aviv, Israel

²¹HL Dodge Department of Physics & Astronomy, University of Oklahoma, 440 W Brooks St, Norman,

ABSTRACT

We report the detections of a giant planet (MARVELS-7b) and a brown dwarf candidate (MARVELS-7c) around the primary star in the close binary system, HD 87646. It is the first close binary system with more than one substellar circum-primary companion discovered to the best of our knowledge. The detection of this giant planet was accomplished using the first multi-object Doppler instrument (KeckET) at the Sloan Digital Sky Survey (SDSS) telescope. Subsequent radial velocity observations using ET at Kitt Peak National Observatory, HRS at HET, the “Classic” spectrograph at the Automatic Spectroscopic Telescope at Fairborn Observatory, and MARVELS from SDSS-III confirmed this giant planet discovery and revealed the existence of a long-period brown dwarf in this binary. HD 87646 is a close binary with a separation of ~ 22 AU between the two stars, estimated using the Hipparcos catalogue and our newly acquired AO image from PALAO on the 200-inch Hale Telescope at Palomar. The primary star in the binary, HD 87646A, has $T_{\text{eff}} = 5770 \pm 80\text{K}$, $\log g = 4.1 \pm 0.1$ and $[\text{Fe}/\text{H}] = -0.17 \pm 0.08$. The derived minimum masses of the two substellar companions of HD 87646A are $12.4 \pm 0.7 M_{\text{Jup}}$ and $57.0 \pm 3.7 M_{\text{Jup}}$. The periods are 13.481 ± 0.001 days and 674 ± 4 days and the measured eccentricities are 0.05 ± 0.02 and 0.50 ± 0.02 respectively. Our dynamical simulations show the system is stable if the binary orbit has a large semi-major axis and a low eccentricity, which can be verified with future astrometry observations.

1. INTRODUCTION

One of the most surprising astronomical developments of the last 25 years has been the discovery of an abundant population of extra-solar planets and brown dwarfs (BDs) (Wolszczan & Frail 1992; Mayor & Queloz 1995; Rebolo et al. 1995; Nakajima et al. 1995).

OK 73019, USA

²²Instituto de Astrofísica de Canarias, E-38205 La Laguna, Tenerife, Spain

²³Universidad de La Laguna, Dpto. Astrofísica, E-38206 La Laguna, Tenerife, Spain

²⁴Fundación Galileo Galilei-IAF, Rambla José Ana Fernández Pérez, 738712 Breña Baja, Tenerife, Spain

²⁵Department of Astronomy, University of Washington, Box 351580, Seattle, WA 98195-1580, USA

²⁶Department of Astrophysics, Princeton University, Princeton, NJ, 08544, USA

Radial velocity (RV) surveys to date have detected over 500 extrasolar planets (Han et al. 2014). The classical planet formation paradigm, that giant planets form and reside only in circular orbits at large distances from their parent stars, works well for our solar system, but not for extrasolar planetary systems. These RV extrasolar planets reveal an astonishing diversity of masses, semi-major axes and eccentricities, from the short period hot Jupiters, to planets in very elongated orbits, to planetary systems with multiple Jupiter-mass planets, to the super-Earth-mass planets with orbital periods of a few days (Butler et al. 2004; McArthur et al. 2004; Santos et al. 2004; Rivera et al. 2005; Lovis et al. 2006; Udry et al. 2006; Howard et al. 2010; Howard et al. 2014). Indeed, if any single statement captures the developments of this field, it is that the observations have continually revealed an unanticipated diversity of planetary systems.

Despite the fact that over 500 known exoplanets have provided important information about planet masses and orbital parameters, many more exoplanets are urgently needed for statistical characterization of emerging classes of planets and tests of detailed theoretical models for planet formation and evolution. A large planet sample is also needed to study the correlation between the presence of planets and stellar properties, such as metallicity, mass, multiplicity, age, evolutionary stage, activity level, and rotation velocity, not to mention the discovery of new planet populations. The growing need of more exoplanet samples triggered the development of multi-object Doppler technology at the University of Florida in 2004-2008. The first full-scale, multi-object Exoplanet Tracker instrument, the W.M. Keck Exoplanet Tracker (KeckET), was constructed in August 2005-February 2006 with Keck Foundation support. It was coupled to a wide field Sloan Digital Sky Survey telescope (SDSS, Gunn et al. 2006) and used for the pilot Multi-Object APO Radial Velocity Exoplanet Large-Area Survey (MARVELS; Ge et al. 2008, 2009; Ge & Eisenstein 2009) in 2006-2007 (Fleming et al. 2010; Eisenstein et al. 2011).

This is the sixth paper in this series examining the low-mass companions around solar type stars from the SDSS-III MARVELS survey (Wisniewski et al. 2012; Fleming et al. 2012; Ma et al. 2013; Jiang et al. 2013; De Lee et al. 2013). In this paper, we present our discovery of two substellar companions, a giant planet (MARVELS-7b) and a brown dwarf (MARVELS-7c), around the primary star in a binary system, HD 87646, from the MARVELS pilot planet survey program. Section 2 reviews our previous knowledge about HD 87646. Section 3 introduces a brief description of the multi-object Doppler instrument and the pilot survey. Section 4 summarizes the survey data processing pipeline, Section 5 describes additional observations of the system, and Section 6 gives details of the results. Section 7 presents the main results and a discussion.

2. HD 87646

The target star, HD 87646, is a bright ($V=8$) G-type star with a fainter K-type stellar companion at a separation of 0.213 arcseconds and a position angle (PA) of 136 degrees according to the Hipparcos and Tycho Catalogues (Perryman 1997). Its Hipparcos parallax of 13.59 ± 1.58 milliarcsecond (mas) places it at a distance of 73.58 ± 9.68 pc. Photometry and high resolution spectroscopic observation of HD 87646A have been obtained by Feltzing & Gustafsson (1998). They obtained a effective temperature of $T_{\text{eff}} = 5961$ K from photometry, and spectroscopically derived $\log g = 4.41$ and $[\text{Fe}/\text{H}] = 0.3$. This star is quite metal rich, prompting Gonzalez et al. (2001) to explicitly recommend that it be observed with precise radial velocity instruments due to the significantly higher probability of discovering hot Jupiter planets around metal rich stars (Fischer & Valenti 2005). While HD 87646 was observed as part of the Geneva Copenhagen Survey (Nordstrom et al. 2008) we are presently unaware of any high precision radial velocity observation, or the star being part of any ongoing surveys.

Such binary systems are challenging for precision radial velocity detection due to the complexity of analyzing spectra from two different stars. While detections of exoplanets in unresolved stellar binaries have been reported before (Konacki 2005), higher precision observations and better cadence have not detected the same signal (Eggenberger et al. 2007). We speculate that this difficulty in detection is the reason this target was not observed in some ongoing surveys, like N2K (Robinson et al. 2006), that target high-metallicity stars. Multi-object surveys do not need to be as selective due to their inherent multiplicity advantage. Binaries may be excluded, but the existence of a few binaries among 60 stars observed simultaneously is not a significant problem. In addition, once observations are well underway there is little advantage gained in removing the target since any replacement target would then only be observed for a few epochs. We will study the impact of spectral contamination from a faint companion star on the RV measurements for our target in Section 6.2. Our study shows that the only substellar companions that can be detected in such close binaries are those massive enough to generate RV signals much larger than the noise induced by the spectral contamination.

3. The Multi-object KeckET pilot survey

The design of KeckET is based on a single object Exoplanet Tracker (ET) design for the KPNO 2.1m telescope (Ge et al. 2003, 2006; Mahadevan et al. 2008). This instrument adopts the dispersed fixed-delay interferometry (DFDI) approach for Doppler measurements (Erskine & Ge 2000; Ge 2002; Ge et al. 2002). Instead of the line centroid shifts in the

high resolution cross-dispersed echelle spectrograph approach, the DFDI method measures the Doppler motion by monitoring the fringe shifts of stellar absorption lines created by a Michelson-type interferometer with a fixed-delay between the two interferometer arms. The measurement of this fixed-delay is described in Wang et al. (2012b,a).

The KeckET instrument consists of 8 subsystems—a multi-object fiber feed, an iodine cell, a fixed-delay interferometer system, a slit, a collimator, a grating, a camera, and a $4k \times 4k$ CCD detector. In addition, it contains four auxiliary subsystems: the interferometer control, an instrument calibration system, a photon flux monitoring system, and a thermal probe and control system. The instrument is fed with 60 fibers with $200 \mu\text{m}$ core diameters, which are coupled to $180 \mu\text{m}$ core diameter short fibers from the SDSS telescope, corresponding to 3 arcsec on the sky at $f/5$ (Ge et al. 2006c). The resolving power for the spectrograph is $R=5100$, and the wavelength coverage is $\sim 900 \text{ \AA}$, centered at 5400 \AA . Details of the instrument design can be found in Ge et al. (2006b), Wan et al. (2006), and Zhao & Ge (2006). KeckET has one spectrograph and one $4k \times 4k$ CCD camera that captures one of the two interferometer outputs, and has a 5.5% detection efficiency from the telescope to the detector without the iodine cell under the typical APO seeing conditions (~ 1.5 arcsec seeing). The CCD camera records fringing spectra from 59 objects in a single exposure.

KeckET was commissioned at the SDSS telescope in Spring 2006. After a few engineering upgrades in Fall 2006, we conducted a pilot planet survey of 700 FGK main sequence stars in 12 fields with $V = 7.6\text{-}12$ to detect new planets in December 2006 to May 2007. A total of 5-25 RV measurements have been obtained for the survey stars. The data were processed by a modified version of data pipeline for the KPNO ET (Ge et al. 2006; van Eyken 2008). The instrument Doppler precision was measured with the day sky scattered light, which offers a stable, homogeneous RV source for simultaneously calibrating the instrument performance for all of the sky fibers. The rms error averaged over the 59 fibers, measured from the dispersion of measurements over a several hour interval in 2006 November, is $6.3 \pm 1.3 \text{ m s}^{-1}$. The corresponding average photon-limit error is $5.5 \pm 0.5 \text{ m s}^{-1}$. The instrument’s precision over longer time intervals has been measured with repeated observations of sky scattered light over a period of 45 days in Fall 2006, and 150 days in Winter/Spring 2007. The rms dispersion of RV measurements of the sky over these periods, after subtracting the photon limiting errors in quadrature, are $11.7 \pm 2.7 \text{ m s}^{-1}$ and $11.3 \pm 2.5 \text{ m s}^{-1}$, respectively.

The instrumental contributions to random measurement errors are mainly caused by inhomogeneous illumination of the slit, image aberration, and the interferometer comb aliasing (sampling on the detector). However, the dominant measurement RV error is produced by the mathematical approximation used for extracting iodine and stellar Doppler signals in the mixed stellar and iodine fringing spectra, which is on the order of 50 m s^{-1} (van Eyken, Ge

& Mahadevan 2010), which is included in the RV errors showing in the data table. Although this error has largely limited our capability of detecting relatively low mass planets, it does not affect the Doppler detection of massive giant planets, brown dwarfs and binaries.

4. Survey Data Processing and RV Results

The pipeline processing steps are described in detail in van Eyken et al. (2004), Ge et al. (2006), Mahadevan et al. (2008) and van Eyken et al. (2010). The data were processed using standard IRAF procedures (Tody 1993), as well as software written in IDL. The images were corrected for biases, dark current, and scattered light and then trimmed, illumination corrected, slant corrected and low-pass filtered. The visibilities (V) and the phases (θ) of the fringes were determined for each channel by fitting a sine wave to each column of pixels in the slit direction. To determine differential velocity shifts the star+iodine data can be considered as a summation of the complex visibilities ($\mathbf{V} = Ve^{i\theta}$) of the relevant star ($V_S e^{i\theta_{S_0}}$) and iodine ($V_I e^{i\theta_{I_0}}$) templates (Erskine 2003; van Eyken et al. 2004, 2010). For small velocity shifts the complex visibility of the data, for each wavelength channel, can be written as

$$V_D e^{i\theta_D} = V_S e^{i\theta_{S_0}} e^{i\theta_S - i\theta_{S_0}} + V_I e^{i\theta_{I_0}} e^{i\theta_I - i\theta_{I_0}}, \quad (1)$$

where V_D , V_S , and V_I are the fringe visibilities for a given wavelength in the star+iodine data, star template, and iodine template respectively, and θ_D , θ_{S_0} , and θ_{I_0} are the corresponding measured phases. In the presence of velocity shifts of the star and instrument drift, the complex visibilities of the star and iodine template best match the data with phase shifts of $\theta_S - \theta_{S_0}$ and $\theta_I - \theta_{I_0}$, respectively. The iodine is a stable reference and the iodine phase shift tracks the instrument drift. The difference between star and iodine shifts is the real phase shift of the star, $\Delta\phi$, corrected for any instrumental drifts

$$\Delta\phi = (\theta_S - \theta_{S_0}) - (\theta_I - \theta_{I_0}). \quad (2)$$

This phase shift can be converted to a velocity shift, Δv , using a known phase-to-velocity scaling factor:

$$\Delta v = \frac{c\lambda}{2\pi d} \Delta\phi, \quad (3)$$

where c is the speed of light, λ is the wavelength and d is the optical delay in the Michelson interferometer. The KeckET data analysis pipeline identifies the shift in phase of the star and iodine templates that are the best match for the data, and uses these phase shifts to calculate the velocity shift of the star relative to the stellar template. Since HD 87646 is a close binary system, we need an additional complex visibility term in equation 1 to account for the contamination of the secondary star. Mathematically this is equivalent to adding a

small noise term $\delta\theta_S$ to the phase of the primary star θ_S (van Eyken, Ge & Mahadevan 2010), which will translate to the measured RV according to equation 3. This noise term depends mainly on the flux ratio of the two stars collected through the fiber and the radial velocity offset between the two stars. Thus this noise term varies slowly between observations. To simplify the RV fitting process, we treat this noise as a constant value and will study its impact on the RV measurements of HD 87646 in section 6.2. In practice, one can try to model the visibility and phase of the secondary star if both star spectra and their flux ratio variations with wavelength are known precisely. This method is not very practical in our current case because of the lack of these information.

We have obtained a total of 16 observations of HD 87646 using KeckET from 2006 December to 2007 June. The radial velocities obtained are listed in Table 1.

5. Follow-up Observations

5.1. KPNO ET RV Observations

Subsequent observations were performed using the Exoplanet Tracker (ET) instrument at KPNO (Ge et al. 2006b). Initial follow-up was performed in November of 2007, which confirmed the variability seen in the KeckET data. Additional data points were obtained at KPNO in 2008 January, 2008 February and 2008 May. The integration time was 35-40 mins in 2007 November and 20 mins in 2008 January, 2008 February and 2008 May.

The data were reduced using software described in Mahadevan et al. (2008) and references therein. See van Eyken, Ge & Mahadevan (2010) for the theory behind the technique. A total of 40 data points were obtained from 2007 November to 2008 May and are listed in Table 2. The observations confirmed the linear trend shown in the KeckET data, which is later to be found due to another substellar companion.

5.2. HET RV observations

Follow-up observations of HD 87646 were conducted with the fiber-fed High Resolution Spectrograph (HRS, Tull 1998) of the Hobby Eberley telescope (HET, Ramsey et al. 1998). The observations were executed in queue scheduled mode (Shetrone et al. 2007), and used a 2 arcsecond fiber and with the HRS slit set to yield a spectral resolution of $R \sim 60,000$. A total of 29 data points were obtained between 2007 December and 2008 March. An iodine cell was inserted into the beam path to yield a fiducial velocity reference. The radial velocities were

Table 1: KeckET Pilot Project Radial Velocities for HD 87646. A total of 16 observations are listed here.

Julian Date (UTC)	Velocity m s^{-1}	Velocity Error m s^{-1}
2454101.86236	21983	52
2454102.02955	22070	54
2454105.97151	21908	53
2454128.81306	21945	52
2454136.77204	20754	52
2454136.80788	20753	51
2454164.75013	20946	53
2454165.74965	20977	52
2454165.78557	20935	52
2454186.65127	22231	51
2454191.72256	21287	53
2454194.73526	21359	53
2454195.72733	21850	52
2454221.62148	21270	51
2454224.61552	23040	52
2454254.63197	21925	55

obtained using the procedure and analysis techniques described in Marcy & Butler (1992). The HRS spectra consisted of 46 echelle orders recorded on the blue CCD (407–592 nm) and 24 orders on the red one (602–784 nm). The spectral data used for RV measurements were extracted from the 17 orders (505–592 nm) in which the I₂ cell superimposed strong absorption lines. The radial velocities obtained are listed in Table 3.

5.3. MARVELS RV observations

HD 87646 was selected as an RV survey target by the MARVELS preselection criterion (Paegert et al. 2015). The star has been monitored at 23 epochs using the MARVELS instrument mounted on the SDSS 2.5m Telescope at APO between 2009 May and 2011 December (Ge et al. 2008, Ma et al. 2013). The MARVELS instrument is a fiber-fed dispersed fixed-delay interferometer instrument capable of observing 60 objects simultaneously and covers a wavelength range of 5000–5700 Å with a resolution of $R \sim 12,000$. The data processing and error estimation algorithm have been described in detail by Thomas et al. (2016). The final differential RV products are included in the SDSS Data Release 12 (Alam et al. 2015) and are presented in Table 4.

5.4. Fairborn RV observations

To investigate the nature of the linear RV trend found in previous RV data, we have obtained additional observations of HD 87646 with a fiber-fed echelle spectrograph situated at the 2 m Automatic Spectroscopic Telescope (AST) in Fairborn Observatory (Eaton & Williamson 2004, 2007). The robotic nature of the AST allowed for high cadence observations, which removed orbital period degeneracies and helped solidify the longer-period companion’s orbit. Through 2011 June the detector was a 2048×4096 SITe ST-002A CCD with 15 micron pixels. The AST echelle spectrograph has 21 orders that cover the wavelength range 4920–7100 Å, and has an average resolution of 0.17 Å. Beginning in 2010 January, several upgrades were made to increase the throughput, sensitivity and flexibility of the AST (Fekel et al. 2013). In the summer of 2011 the SITe CCD detector and dewar were replaced with a Fairchild 486 CCD having 4K×4K 15 micron pixels, which required a new readout electronics package, and a new dewar with a Cryotiger refrigeration system. The echelle spectrograms that were obtained with this new detector have 48 orders, covering the wavelength range 3800–8260 Å. The data reduction and radial velocity measurements are discussed in Eaton & Williamson (2007). A total of 135 data points were obtained from 2009 March through 2013 October and are listed in Table 5. With these additional RV data,

Table 2: KPNO ET Radial Velocities for HD 87646. This table is available in its entirety in the online journal. There are a total of 40 observations. A portion is shown here for guidance regarding its form and content.

Julian Date (UTC)	Velocity m s ⁻¹	Velocity Error m s ⁻¹
2454425.90567	19968	51
2454425.98306	19869	51
2454427.90591	19207	52
2454427.98285	19219	53
2454428.98821	19896	52
2454430.00529	20101	54
2454431.90248	19143	54
2454431.97582	19159	55
2454491.88155	20158	55
2454491.93285	20230	54

Table 3: HET Radial Velocities for HD 87646. This table is available in its entirety in the online journal. There are a total of 29 observations. A portion is shown here for guidance regarding its form and content.

Julian Date (UTC)	Velocity m s ⁻¹	Velocity Error m s ⁻¹
2454454.85471	-192.5	44.0
2454454.85762	-201.0	34.3
2454455.86358	198.4	35.6
2454455.86528	192.1	31.8
2454458.86351	-746.7	12.9
2454461.84553	-1508.8	37.3
2454462.82117	-1191.1	18.6
2454463.83110	-678.3	12.3
2454470.81807	144.1	21.8
2454473.78993	-1332.5	17.0

we were able to detect the turnaround of the previous identified linear RV trend and start to uncover the second substellar companion’s orbit.

5.5. TNG high resolution spectroscopy

A total of nine high-resolution spectra ($R = 164,000$) of HD 87646 were obtained with the SARG spectrograph on the 3.5-m TNG telescope at La Palma on 2008 March 21, 22, 28, April 03 and April 11. These data were used to monitor line bisector variations, to determine stellar properties (metallicity, $\log g$, T_{eff} and $v \sin i$), and to search for evidence of a second set of lines in the system. The typical signal-to-noise ratio (S/N) for each spectrum is about 150 per resolution element around 5500\AA .

5.6. KPNO EXPERT high resolution spectroscopy

We also obtained spectroscopic observations of HD 87646 from the 2.1m telescope at Kitt Peak National Observatory using the $R = 30,000$ Direct Echelle Mode of the EXPERT spectrograph (Ge et al. 2010). A total of seven EXPERT spectra were acquired between 2014 Feb to 2014 June. The exposure time for each observation ranged from 20-40 minutes, yielding an $S/N \sim 250$ per resolution element around 5500\AA .

5.7. Lucky imaging

On 2008 May 29, high angular resolution lucky images of HD 87646 were obtained with the FastCam instrument (Oscoz et al. 2008) on the 2.5-meter Nordic Optical Telescope at the Roque de los Muchachos Observatory in La Palma (Spain). Five data cubes of 1000 images each were obtained using the I-band filter. Individual exposure times were 30 ms for each image. High spatial resolution was obtained by combining the best 1% of the images. Fig. 1 shows the processed image. The image scale was $30.95 \pm 0.05 \text{ mas pixel}^{-1}$. In this figure the secondary star HD 87646B in this binary system is visible. The point spread function (PSF) of the star has a full width half maximum (FWHM) value of $0.11''$.

Table 4: MARVELS Radial Velocities for HD 87646. This table is available in its entirety in the online journal. There are a total of 23 observations. A portion is shown here for guidance regarding its form and content.

Julian Date (UTC)	Velocity m s^{-1}	Velocity Error m s^{-1}
2454960.63450	121	41
2454961.63480	33	41
2455193.99281	-652	51
2455197.91351	-529	43
2455223.8140	-186	46
2455284.82871	-1785	53

Table 5: Fairborn Radial Velocities for HD 87646. This table is available in its entirety in the online journal. There are a total of 135 observations. A portion is shown here for guidance regarding its form and content.

Julian Date (UTC)	Velocity (ms^{-1})	Velocity Error (ms^{-1})
2454903.7521	21690	212
2454904.8249	20810	289
2454905.6178	21580	187
2454906.7753	21470	258
2454908.7537	21290	142
2454909.7757	21530	179
2454910.7670	21600	342
2454911.7909	22720	171
2454913.7546	22740	214
2454914.7619	22140	217

5.8. Palomar AO imaging

On 2009 June 4, we acquired high resolution AO images of the binary star system HD 87646 from PALAO on the 200-inch Hale Telescope at Palomar. Data sets were taken in the J and K bands. The AO system was running at 500 Hz. The seeing was roughly 1.3" in K band. We also observed a calibrator star and subtracted the K-band's PSF, which improved sensitivity by a factor of a few. The utility of PSF subtraction is limited, in this case, by the difference in stellar spectral types, since the filters are broad.

Images were flat-fielded, background subtracted and cleaned; the final images are displayed on a logarithmic scale in Fig. 2 with a scale of 25 mas pixel⁻¹. The binary system is well-resolved in both bands. The angular separation is measured to be 401 ± 12 mas, nearly twice that quoted from the Hipparcos and Tycho Catalogues (Perryman 1997). The position angle is $69.8^\circ \pm 0.5^\circ$. There is no evidence in the high resolution images for a tertiary (stellar) companion. The J and K-band brightness ratios of the two stars are 6.18 ± 0.12 and 5.82 ± 0.10 , respectively. We can not use these ratios and their error bars to put a meaningful constraint on the optical band flux ratio because the spectral energy distribution (SED) curve slope is basically flat in the J and K-bands, but very sharp in the optical band.

5.9. APT Photometry

Photometry of HD 87646 was obtained in the Stromgren *b* and *y* bands between 2007 December and 2015 June with the T12 0.8-m Automatic Photoelectric Telescope (APT) at Fairborn Observatory in Arizona. Our primary goal with photometry is to detect if the companions transit the primary star. The data were processed using software described in Henry (1999). The measurements have a typical accuracy of ~ 0.001 mag.

6. Results

6.1. Stellar Parameters

The SARG spectra taken at TNG without the iodine cell were used to derive the stellar parameters. HD 87646 is flagged as a binary in the Hipparcos and Tycho Catalogues (Perryman 1997), with a Hipparcos magnitude (a broad band V filter) difference between the primary and secondary to be 2.66 ± 0.96 mag. Taking into account the binary nature of the object, we explored possible combinations of stellar parameters for the primary and secondary. The SED and the colors change slightly due to the secondary contribution; however,

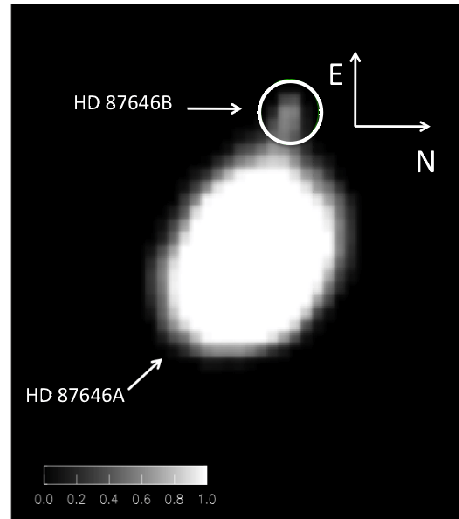


Fig. 1.— A Lucky image of the HD 87646 system, generated by processing and co-adding only the best 1% of the images taken by FastCam on the 2.5-meter Nordic Optical Telescope at the Roque de los Muchachos Observatory in La Palma, Spain. The secondary star, HD 87646B, is highlighted by the solid white circle. The image has a scale of $31 \text{ mas pixel}^{-1}$ and the star PSF has a FWHM of $0.11''$.

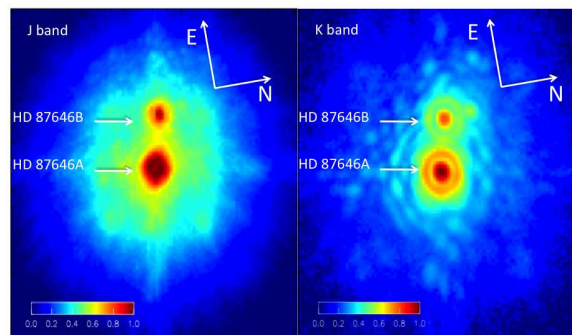


Fig. 2.— J and K band AO imaging of HD 87646 taken at Palomar observatory. The images are displayed on a logarithmic scale, which show the two stars have a separation of $401 \pm 12 \text{ mas}$. The images have a scale of $25 \text{ mas pixel}^{-1}$. The FWHMs are 70 mas and 120 mas for J and K band images respectively.

the normalized spectra show minor changes, only affecting the wings of strong lines (e.g the Mgb lines, Fig. 3). The equivalent widths of most weak lines are essentially unchanged, so we used Fe I and FeII lines with equivalent widths below 140mÅ and performed traditional spectroscopic analysis.

We use the latest MARCS model atmospheres (Gustafsson et al. 2008) for the analysis. Generation of synthetic spectra and the line analysis were performed using the turbospectrum code (Alvarez & Plez 1998), which employs line broadening according to the prescription of Barklem & O’Mara (1998). The line lists used are drawn from a variety of sources. Atomic lines are taken mainly from the VALD database (Kupka et al. 1999). The molecular species CH, CN, OH, CaH and TiO are provided by B. Plez (see Plez & Cohen 2005), while the NH, MgH and C₂ molecules are from the Kurucz line lists. The solar abundances used here are the same as Asplund (2005). We use FeI excitation equilibrium and derived an effective temperature $T_{\text{eff}} = 5770 \pm 80 \text{K}$, which is slightly lower than the effective temperature derived from photometry (Feltzing & Gustafsson 1998). The H α and H β wings also agree better for this lower T_{eff} value. We find $\log g = 4.1 \pm 0.1$, based on ionization equilibrium of FeI and FeII lines and by fitting the wings of the Mgb lines, which agrees with the previous estimates. A microturbulence value of 1.8 km s^{-1} is derived by forcing weak and strong FeI lines to yield the same abundances. We are not able to confirm the super solar metallicity of this object (Feltzing & Gustafsson 1998); we derived $[\text{Fe}/\text{H}] = -0.17 \pm 0.08$. When we adopt the same T_{eff} and microturbulence as Feltzing & Gustafsson (1998), we obtain the same metallicity value $[\text{Fe}/\text{H}] = 0.3$, but with a large slope in the excitation potential versus FeI abundance and reduced equivalent width versus FeI abundance. The derived stellar parameters are summarized in Table 6.

We attempted to place constraints on the secondary star by fitting the Balmer line and Mgb line wings. Based on the Hipparcos data, which suggest a Hipparcos magnitude

Table 6: Parameters of the Star HD 87646A

Parameter	Value
T_{eff}	$5770 \pm 80 \text{ K}$
$\log(g)$	4.1 ± 0.1
$[\text{Fe}/\text{H}]$	-0.17 ± 0.08
$V \sin i$	7.5 kms^{-1}
ξ_t	1.8 kms^{-1}
Mass	$1.12 \pm 0.09 M_{\odot}$
Radius	$1.55 \pm 0.22 R_{\odot}$

difference between the primary and secondary 2.66 ± 0.96 mag, the secondary has a flux contribution of 8-10% with respect to the primary. We synthesized binary spectra with a G dwarf primary and a K dwarf secondary, with 10% and 50% flux contribution from the secondary. The binary spectrum synthesis results are consistent with the Hipparcos data with 10% contribution from the secondary. We cannot place better estimates based on the spectral line profiles because of the large errors in the continuum normalization of these lines, since they spread over the entire echelle order.

We use the empirical polynomial relations of Torres, Andersen & Giménez (2010) to estimate the mass and radius of the primary star, HD 87646A, from T_{eff} , $\log(g)$, and $[\text{Fe}/\text{H}]$. These relations were derived from a sample of eclipsing binaries with precisely measured masses and radii. We estimate the uncertainties in M_* and R_* by propagating the uncertainties in T_{eff} , $\log(g)$, and $[\text{Fe}/\text{H}]$ using the covariance matrices of the Torres, Andersen & Giménez (2010) relations (kindly provided by G. Torres). Since the polynomial relations of Torres, Andersen & Giménez (2010) were derived empirically, the relations were subject to some intrinsic scatter, which we add in quadrature to the uncertainties propagated from the stellar parameter measurements ($\sigma_{\log m} = 0.027$ and $\sigma_{\log r} = 0.014$; Torres, Andersen & Giménez 2010). The final stellar mass and radius values obtained are $M_* = 1.12 \pm 0.09 M_{\odot}$ and $R_* = 1.55 \pm 0.22 R_{\odot}$.

6.2. Systematic RV Errors Due to the Blended Binary Spectrum

HD 87646 is a binary system, and contamination of the primary star’s spectrum by the secondary star leads to an increased RV jitter by interfering with the analysis pipeline. In this section we investigate the possible systematic RV errors caused by the blended binary spectra using simulations. Since our RV observations were produced by two different kinds of spectrographs, we decided to perform two simulations, one for the DFDI instruments, including KeckET, KPNO ET, and MARVELS, and the other for traditional echelle spectrographs, including HRS at HET and the AST fiber-fed echelle spectrograph at Fairborn. In both simulations, we first create a set of stellar spectra by combining a G-type star (for the primary) and a K-type (for the secondary) star spectra with varying radial velocities for both stars. Then we calculate the differential radial velocities for the G-star from the simulated spectra. The differences between the output G-star RVs and input G-star RVs are the RV errors caused by secondary star spectra contamination. Both simulations yield similar RV errors on the order of 200 m s^{-1} . We expect to see this level of systematic error and will include it in the RV ‘jitter’ term when we perform the RV curve fitting in the next section. Traditionally the ‘jitter’ term used to denote any RV noise caused by stellar activity; our ‘jitter’ term also contains the RV noise caused by blended binary spectra.

6.3. RV curve fitting and orbital parameters

We have performed a Markov Chain Monte Carlo (MCMC) analyses of the combined RV observations from KeckET, ET, HET, MARVELS and Fairborn instruments. In this analyses, we initially used a one planet RV model to fit our RV observations, and later found that there is another strong periodic RV signal in the RV residuals. We then adopted a two object (a planet and a brown dwarf) RV model to fit our RV data. The RV model details are presented in §2 of Gregory (2007). We have attempted to add in another planet to fit our RV data around the third peak in the periodogram. The addition of another planet did not significantly improve our RV fitting. And combining with the fact that the newly added planet has a period half of the first giant planet, and eccentricity of 0.99, we consider it as an alias and over-fit of the noise. Thus we have rejected the RV model with a three substellar companions. Throughout the paper, we only present and discuss the RV model with two substellar companions.

Each state in the Markov chain is described by the parameter set

$$\vec{\theta} = \{P_1, K_1, e_1, \omega_1, M_1, P_2, K_2, e_2, \omega_2, M_2, C_i, \sigma_{\text{jitter}}\}, \quad (4)$$

where P_1 and P_2 are orbital periods, K_1 and K_2 are the radial velocity semi-amplitudes, e_1 and e_2 are the orbital eccentricities, ω_1 and ω_2 are the arguments of periastron, M_1 and M_2 are the mean anomalies at chosen epoch (τ), C_i is constant velocity offset between the differential RV data shown in Tables 1, 2, 3, 4, and 5 and the zero-point of the Keplerian RV model ($i = 1$ for KeckET observations, $i = 2$ for KPNO ET observations, $i = 3$ for HET observations, $i = 4$ for MARVELS observations, and $i = 5$ for Fairborn observations), and σ_{jitter} is the “jitter” parameter. The jitter parameter describes any excess noise, including both astrophysical noise (e.g. stellar oscillation, stellar spots; Wright 2005), any instrument noise not accounted for in the quoted measurement uncertainties and systematic RV errors from analyzing blended binary spectra discussed in the last section. We use standard priors for each parameter (see Gregory 2007). The prior is uniform in the logarithm of the orbital period (P_1 and P_2) from 1 to 5000 days. For K_1 , K_2 and σ_{jitter} we use a modified Jefferys prior which takes the form of $p(x) = (x + x_o)^{-1}[\log(1 + x_{\text{max}}/x_o)]^{-1}$, where $x_o = 0.1 \text{ m s}^{-1}$ and $x_{\text{max}} = 2128 \text{ m s}^{-1}$ (Gregory 2005). Priors for e_1 and e_2 are uniform between zero and unity. Priors for ω_1 , ω_2 , M_1 and M_2 are uniform between zero and 2π . For C_i , the priors are uniform between $\min(v_i) - 5 \text{ km s}^{-1}$ and $\max(v_i) + 5 \text{ km s}^{-1}$, where v_i are the set of radial velocities obtained from each of the four instruments ($i = 1$ for KeckET observations, $i = 2$ for KPNO ET observations, $i = 3$ for HET observations, $i = 4$ for MARVELS observation, and $i = 5$ for Fairborn observations). We verified that the chains did not approach the limiting value of P_1 , P_2 , K_1 , K_2 and σ_{jitter} .

Following Ford (2006), we adopt a likelihood (i.e., conditional probability of making the specified measurements given a particular set of model parameters) of

$$p(v|\vec{\theta}, M) \propto \prod_k \frac{\exp[-(v_{k,\theta} - v_k)^2/2(\sigma_{k,obs}^2 + \sigma_{jitter}^2)]}{\sqrt{\sigma_{k,obs}^2 + \sigma_{jitter}^2}}, \quad (5)$$

where v_k is observed radial velocity at time t_k , $v_{k,\theta}$ is the model velocity at time t_k given the model parameters $\vec{\theta}$, and $\sigma_{k,obs}$ is the measurement uncertainty for the radial velocity observation at time t_k .

We combine the Markov chains described above to estimate the joint posterior probability distribution for the orbital model for HD 87646. In Table 7 we report the median value and an uncertainty estimate for each model parameter based on the marginal posterior probability distributions. The uncertainties are calculated as the standard deviation about the mean value from the combined posterior sample. Since the shape of the marginal posterior distribution is roughly similar to a multivariate normal distribution, the median value plus or minus the reported uncertainty roughly corresponds to a 68.3% credible interval. In the same table, we also reported the rms of the RV fitting residuals for the five different RV instruments used here, which are $\text{rms}_1 = 245 \text{ m s}^{-1}$ for KeckET, $\text{rms}_2 = 248 \text{ m s}^{-1}$ for KPNO ET, $\text{rms}_3 = 261 \text{ m s}^{-1}$ for HET, $\text{rms}_4 = 270 \text{ m s}^{-1}$ for MARVELS, and $\text{rms}_5 = 312 \text{ m s}^{-1}$ for Fairborn RV observations.

This two-Keplerian orbital solution is shown in Figs 4 and 5 together with the KeckET, HET, KPNO ET, Fairborn and MARVELS RV data. The residuals in these two plots can not be explained only by the errors in our RV data. A stellar jitter term $\sigma_{jitter} = 240 \pm 12 \text{ m s}^{-1}$ is required in our fitting to explain these residuals. As discussed in the last section, most of the ‘jitter’ noise arises from our data pipeline handling the blended binary spectra instead of a single star spectra. We also did an MCMC analysis using two ‘jitter’ noise terms, one for DFDI instruments and the other one for echelle spectrographs, and find the orbital parameters for the giant planet candidate and the BD candidate are barely changed within the error bars. So to keep it simple, we choose to use one ‘jitter’ term for all our RV observations from different instruments.

HD 87646 is a binary system, so we have done another MCMC analysis by including a linear RV trend ($v_{\text{trend}} \times (t - t_0)$) to the two-objects RV model used above. This linear RV trend is used to account for the perturbation of the primary star induced by the gravitational force of the secondary star. We note here that the offsets between different data sets will hinder the modeling of this linear trend as there is expected strong correlation between the offsets and this linear trend. Our new RV fitting yields orbital parameters for the two sub-stellar companions in addition to a linear RV trend of $v_{\text{trend}} = -12 \pm 18 \text{ m s}^{-1} \text{ yr}$, which are summarized in Table 8. Since all the main orbital parameters of the two sub-stellar

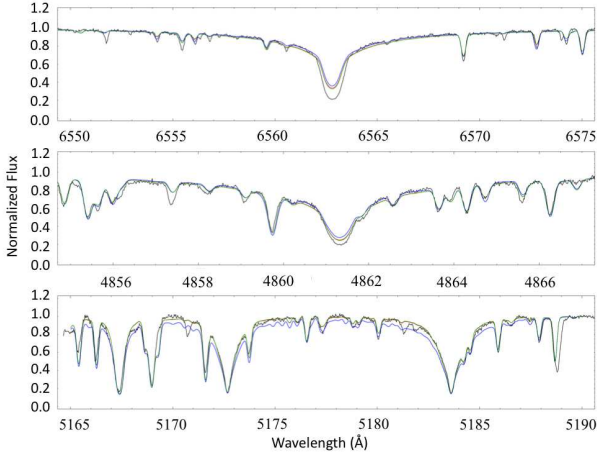


Fig. 3.— High resolution TNG spectra of HD 87646 centered around $H\alpha$, $H\beta$ and Mgb lines (black lines). The three other lines correspond to synthetic spectra for a binary with a G dwarf primary ($T_{\text{eff}} = 5770$ K, $\log g = 4.1$, $[\text{Fe}/\text{H}] = -0.17$, Microturbulence = 1.8 km s^{-1} and $V \sin i = 7.5 \text{ km s}^{-1}$) and a K dwarf secondary ($T_{\text{eff}} = 4000$ K, $\log g = 5.0$). The green, red and blue lines correspond to a 0%, 10% and 50% flux contribution from the secondary to the whole binary.

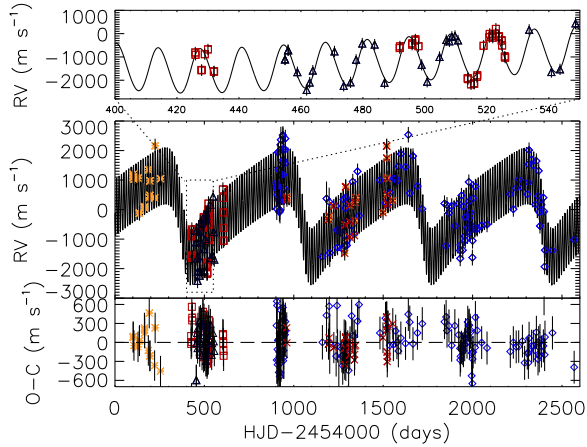


Fig. 4.— *Top*: Expanded section of the middle panel plot (the dotted rectangular region) to show the short-period giant planet signal in the two-Keplerian RV model. *Middle*: Radial velocity observations of HD 87646 with the two-Keplerian model. *Bottom*: RV residuals of the two-Keplerian orbit model. Each panel shows radial velocity observations from KeckET (yellow stars), HET (black triangles), KPNO ET (red squares), Fairborn (blue diamonds), and MARVELS (red cross).

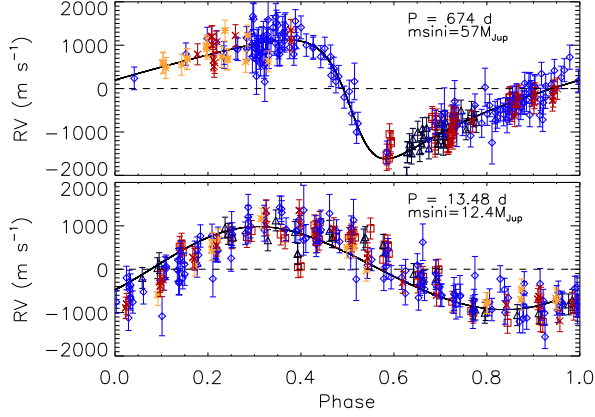


Fig. 5.— Phased RV curves for the two signals in the two-Keplerian RV model. In each case, the contribution of the other signal was subtracted. Each panel shows radial velocity observations from KeckET (yellow stars), HET (black triangles), KPNO ET (red squares), Fairborn (blue diamonds), and MARVELS (red cross).

Table 7: Orbital Parameters for HD 87646b and HD 87646c

Parameter	HD 87646b	HD 87646c
Minimum Mass	$12.4 \pm 0.7 M_{\text{Jup}}$	$57.0 \pm 3.7 M_{\text{Jup}}$
a	$0.117 \pm 0.003 \text{ AU}$	$1.58 \pm 0.04 \text{ AU}$
K	$956 \pm 25 \text{ m s}^{-1}$	$1370 \pm 54 \text{ m s}^{-1}$
P	$13.481 \pm 0.001 \text{ d}$	$674 \pm 4 \text{ d}$
e	0.05 ± 0.02	0.50 ± 0.02
ω (radians)	5.20 ± 0.52	1.95 ± 0.06
$T_{\text{prediction for transit}} (\text{JD}_{\text{UTC}})$	$2454093.85 \pm 0.12 \text{ d}$	
$T_{\text{periastron}} (\text{JD}_{\text{UTC}})$	$2454088.3 \pm 1.1 \text{ d}$	$2453707 \pm 9 \text{ d}$
σ_{jitter}	$240 \pm 12 \text{ m s}^{-1}$	
C_1	$20.878 \pm 0.050 \text{ km s}^{-1}$	
C_2	$20.777 \pm 0.090 \text{ km s}^{-1}$	
C_3	$0.908 \pm 0.080 \text{ km s}^{-1}$	
C_4	$-0.306 \pm 0.050 \text{ km s}^{-1}$	
C_5	$20.786 \pm 0.070 \text{ km s}^{-1}$	
rms_1	245 m s^{-1}	
rms_2	248 m s^{-1}	
rms_3	261 m s^{-1}	
rms_4	270 m s^{-1}	
rms_5	312 m s^{-1}	

Table 8: Orbital Parameters for HD 87646b and HD 87646c with a Linear RV Trend

Parameter	HD 87646b	HD 87646c
Minimum Mass	$12.4 \pm 0.7 M_{\text{Jup}}$	$57.0 \pm 3.7 M_{\text{Jup}}$
a	$0.117 \pm 0.003 \text{ AU}$	$1.58 \pm 0.04 \text{ AU}$
K	$954 \pm 24 \text{ m s}^{-1}$	$1370 \pm 56 \text{ m s}^{-1}$
P	$13.481 \pm 0.001 \text{ d}$	$673 \pm 4 \text{ d}$
e	0.05 ± 0.02	0.50 ± 0.02
ω (radians)	5.18 ± 0.48	1.95 ± 0.06
$T_{\text{prediction for transit}} (\text{JD}_{\text{UTC}})$	$2454093.86 \pm 0.14 \text{ d}$	
$T_{\text{periastron}} (\text{JD}_{\text{UTC}})$	$2454088.2 \pm 1.0 \text{ d}$	$2453709 \pm 8 \text{ d}$
v_{trend}	$-12 \pm 18 \text{ m s}^{-1} \text{ yr}^{-1}$	
σ_{jitter}	$240 \pm 13 \text{ m s}^{-1}$	
C_1	$20.89 \pm 0.070 \text{ km s}^{-1}$	
C_2	$20.79 \pm 0.10 \text{ km s}^{-1}$	
C_3	$0.92 \pm 0.09 \text{ km s}^{-1}$	
C_4	$-0.262 \pm 0.06 \text{ km s}^{-1}$	
C_5	$20.838 \pm 0.09 \text{ km s}^{-1}$	
rms ₁	246 m s^{-1}	
rms ₂	248 m s^{-1}	
rms ₃	261 m s^{-1}	
rms ₄	269 m s^{-1}	
rms ₅	312 m s^{-1}	

companions are barely changed within their respect error bars and the strong correlation between this RV trend and telescopes RV offsets, we decide to keep using the numbers present in Table 7 throughout this paper. This linear trend is not significant, which means it is more likely that either the secondary star is close to its ascending or descending node during 2008-2013, or this binary is on a relatively low-inclination (face on) orbit. It is not possible for us to distinguish these two scenarios using our current data. Future high precision astrometry observations, like GAIA, will help to solve this binary orbital problem. We also want to note here that this linear trend is not exact the real RV trend of the primary star induced by the gravitational perturbation of the secondary star because of the secondary star’s spectral contamination. It is close to $\sim 70\text{-}80\%$ of the real trend value assuming the flux ratio of the two stars is ~ 10 in the optical band and mass ratio is ~ 2 .

6.4. Line Bisector Analysis

Santos et al. (2002) found small radial velocity variations and line asymmetries for the star HD 41004, which is a visual binary and is unresolved at the spectrograph. It was initially thought to have a planetary companion around the primary star, but from the line bisector analysis they were able to infer a possible brown dwarf orbiting the secondary star instead of a planet orbiting the primary star. Their conclusions were subsequently corroborated by Zucker et al. (2003).

Similar to HD 41004, HD 87646 is also a binary system with a small angular separation ($0.4''$), which renders the spectrum a blended spectrum of the two stellar components. Following the same philosophy of Santos et al. (2002), we performed a bisector analysis for HD 87646 to determine from which star in the binary system the RV signal was produced. We have analyzed spectra taken at the Kitt peak 2m telescope using EXPERT (Ge et al. 2010). Spectra were reduced using an IDL pipeline modified from an early version described in Wang (2012). Frames were trimmed, bias subtracted, flat-field corrected, aperture-traced, and extracted. Cross-Correlation Functions (CCFs) are derived by cross-correlation with a spectral mask from the wavelength range $4900 - 6300\text{\AA}$. Then we compute the bisector velocity for 10 different levels of the CCF. The values for the upper (near continuum) and lower bisector points are averaged and subtracted. The resulting quantity (the Bisector Inverse Slope, BIS) can be used to measure the line bisector variations (Queloz et al. 2001). The result of the bisector analysis is presented in Fig. 6, which demonstrates that the BIS varies in phase with the radial velocity.

We then created two simulations following Santos et al. (2002), one by assuming a giant planet orbiting the primary star of the binary (solid line in Fig. 6) and the other by assuming

a heavier BD orbiting the secondary star (dotted line in Fig. 6). Both scenarios can explain the RV curve seen for HD 87646, but clearly only the one in which the giant planet is orbiting the primary star (solid line in Fig. 6) is consistent with the BIS analysis. Our conclusion from the BIS analysis is that the 13.5-day period giant planet is orbiting the primary star HD 87646A.

6.5. Photometry results

The top panel of Fig. 7 presents all 1077 photometric observations plotted against the latest transit ephemeris of HD 87646a: $T_c = 2454093.85$ d, $P = 13.481$ d. The differential magnitudes are measured against the mean of three comparison stars to improve precision. The standard deviation of these data from their mean is 0.0014 mag. A least-squares sine-curve fit to the phased data yields a full amplitude of 0.000089 ± 0.000065 mag. There is no detectable brightness variation on the short period radial velocity period; this result supports the interpretation that the observed radial velocity variations are caused by a companion.

The bottom panel of Fig. 7 is similar to the top panel except that it displays only the data within ± 0.1 phase units from the predicted transit time. We also show the predicted central transit, phased at 0.5, for a duration of 0.21 days or ~ 0.015 units of phase and a depth of 0.5% or ~ 0.005 mag (Kane & von Braun 2008). The $\pm 1\sigma$ uncertainty in the transit window timing is indicated by the two vertical dotted lines. There are 1005 observation that lie outside the predicted transit window, which have a mean of 0.99998 ± 0.00005 mag and 72 observations that fell within the transit window have a mean of 1.0003 ± 0.0002 mag. The difference between these two mean brightness is 0.0003 ± 0.0002 mag. Full transits with a predicted depth ~ 0.005 mag are excluded by the photometry at the predicted transit time.

6.6. Companion Inclination & Mass Estimate

The mass function is related to the observed period, eccentricity and radial velocity semi-amplitude as:

$$\frac{(m \sin i)^3}{(M_* + m)^2} = \frac{P(1 - e^2)^{\frac{3}{2}} K^3}{2\pi G} \quad (6)$$

where M_* is the mass of the primary and m the mass of the companions. Since the first companion is known not to transit the star, we cannot break the degeneracy of mass and $\sin i$ with radial velocity observations alone. Using the derived stellar mass ($1.12M_\odot$) for the primary with the orbital parameters determined from the radial velocity (Table 7) we determine that the minimum mass of the inner companion for an edge-on orbit ($\sin i = 1$)

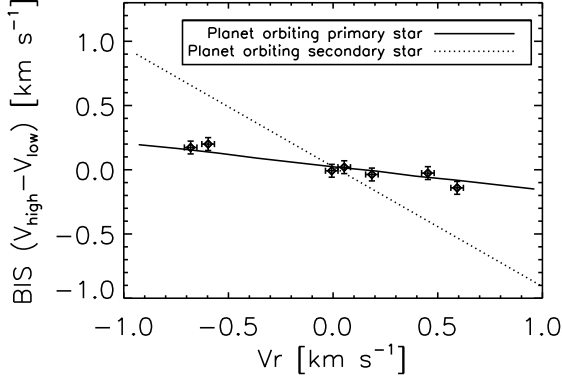


Fig. 6.— Measured radial-velocity vs. BIS from EXPERT spectroscopic data for HD 87646. The solid and dotted lines show simulation results when assuming a giant planet orbiting the primary star and the secondary star, respectively.

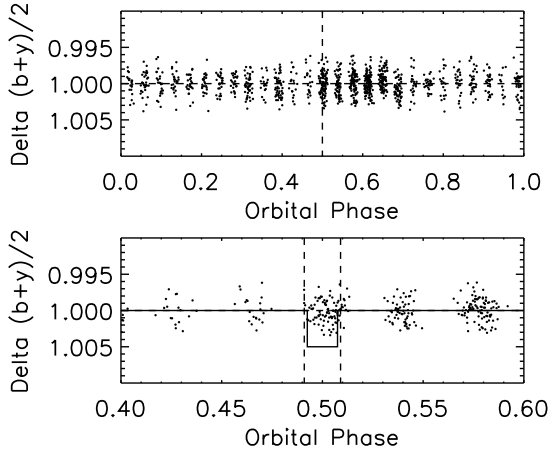


Fig. 7.— Top: the 1077 differential magnitudes of HD 87646 phased to the period of the giant planet HD 87646Ab, taken by the 0.8m APT from 2008-2015. The horizontal dashed line corresponds to the mean brightness level of the 1077 observations. The vertical dashed line marks the expected time of mid-transit. Bottom: an expanded portion of the top plot, centered on the predicted central transit window. The solid curve shows the predicted central transit, with a depth of 0.005 mags and duration of 0.015 units of phase. The $\pm 1\sigma$ uncertainty in the transit window timing is indicated by the two vertical dotted lines.

is $12.4 \pm 0.7 M_{\text{Jup}}$. This mass is quite close to the deuterium burning limit, and the detected companion is likely burning deuterium, although its minimum mass places it in the giant planet regime. The second companion’s minimum mass when assuming an edge-on orbit is $57.0 \pm 3.7 M_{\text{Jup}}$, which falls right into the brown dwarf regime.

7. Summary and Discussion

7.1. Summary of the main results

Our SDSS MARVELS pilot survey and additional observations at the HET, KPNO 2.1m telescope, and Fairborn observatory confirm the detection of two massive substellar companions in a close binary system HD 87646. The first companion, HD 87646Ab, has a minimum mass of $12.4 \pm 0.7 M_{\text{Jup}}$, period of 13.481 ± 0.001 days and eccentricity of 0.05 ± 0.02 . The measured eccentricity is in line with other short period giant planets in binaries (e.g., Eggenberger et al. 2007). This companion is likely to be a giant planet or a brown dwarf, depending on its inclination angle. Our bisector analysis has shown that this companion is in orbit around the primary star. The second companion has a minimum mass of $57 \pm 3.7 M_{\text{Jup}}$, period of 674 ± 4 days and eccentricity of 0.50 ± 0.02 . This companion is likely to be a brown dwarf. Ma & Ge (2014) have found long period high mass ($>42 M_{\text{Jup}}$) BDs tend to have higher eccentricities. This new BD is consistent with this trend.

This is the eleventh detection of a substellar companion(s) in a binary system with separation of only about 20 AU. The other ten systems are Gliese 86 (Queloz et al. 2000; Murgauer & Newhauser 2005; Lagrange et al. 2006), γ Cephei (Hatzes et al. 2003), HD 41004 (Zucker et al. 2003, 2004), HD 188753 (Konacki 2005), HD 176051 (Muterspaugh et al. 2010), HD 126614 (Howard et al. 2010), α Centauri (Dumusque et al. 2012), HD 196885 (Correia et al. 2008), OGLE-2013-BLG-0341 (Gould et al. 2014) and HD 59686 (Ortiz et al. 2016). However, Eggenberger et al. (2007) did not confirm the planet in HD 188753, and Rajpaul, Aigrain, & Roberts (2016) suggest the planet signal discovered from α Centauri B is not from a real planet, but from the observation window function. To the best of our knowledge, HD 87646A is the first multiple planet/BD system detected in such close binaries.

7.2. Dynamical Stability of HD 87646

In this section we will discuss the dynamical stability of the binary system HD 87646. First we have collected observational data of HD 87646 from the literature (Horch et al. 2008, Hartkopf & Mason 2009, Horch et al. 2010, Balega et al. 2013) and combined them with our

AO data to constrain the binary orbit of HD 87646. Our best fitting binary orbital solution (solid line) and the observational data (black dots) are shown in Fig. 8. The best fitting parameters are $P = 51.6$ yr, $e = 0.54$ and $a = 0.26$ arcsec. At a distance of 73.58 ± 9.68 pc, this angular separation corresponds to a binary semi-major axis of 19 ± 2 AU. Since the observational data only cover less than half of the binary orbit, these fitting parameters are very preliminary. There are many previous cases for which binary orbital parameters were revised significantly with new and better astrometry measurements, especially when the binary orbit is not completely covered by astrometry observations yet (Hartkopf & Mason 2009). Using the same classification of visual binaries as that in Hartkopf, Mason & Worley (2001) Hartkopf et al. (2001) for the Catalog of Visual Binary, our orbital solution has a grade 4 (1 = definitive, 2 = good, 3 = reliable, 4 = preliminary, 5 = indeterminate) and formal errors of the orbital solution were considered to have little meaning.

We then performed a numerical simulation of the binary system including the giant planet and brown dwarf discovered in this paper. The binary-planetary-brown dwarf system of HD 87646 was integrated numerically using the Bulirsch-Stoer integrator of the N-body integration package Mercury (Chambers 1999). For each simulation, we tested the dynamical stability of this system given the semi-major axis (a_B) and eccentricity (e_B) of the binary system up to a million years. We have assumed the giant planet, brown dwarf and binary to be coplanar. The results are shown in Fig. 9. There is a stable zone in the binary a_B - e_B diagram. We have scaled the error bars of these astrometry data to force the best orbital fit to have a reduced chi-squared $\chi_{\text{red}}^2 = 1$ and then over-plotted the binary orbital parameter fit from astrometry data with $\max \chi_{\text{red}}^2 = 2$ in Fig. 9. The big uncertainty of the binary orbital fitting from astrometry data arises from the big error bar (~ 0.1 arcsec) of the 1991 Hipparcos data point. We want to point out there is another caveat of this plot, which is from our scaling of the error bars of all the astrometry data points. These data are from 5 different previous observation programs and scaling all of them together to make the best fit have a $\chi_{\text{red}}^2 = 1$ can be problematic. The main conclusion from the simulation study and astrometry data fitting is, with a large binary semi-major axis ($a_B > 17$ AU) and a relatively low binary eccentricity ($e_B < (a_B - 17) \times 0.57 + 0.2$), the binary-planet-brown dwarf system discovered in this paper is stable.

7.3. Nature of the system and its formation and evolution

HD 87646 is the first known system to have two massive substellar objects orbiting a star in a close binary system. Interestingly, the masses of these two substellar objects are close to the minimum masses for burning deuterium ($\sim 13 M_{\text{Jup}}$, Spiegel et al. 2011)

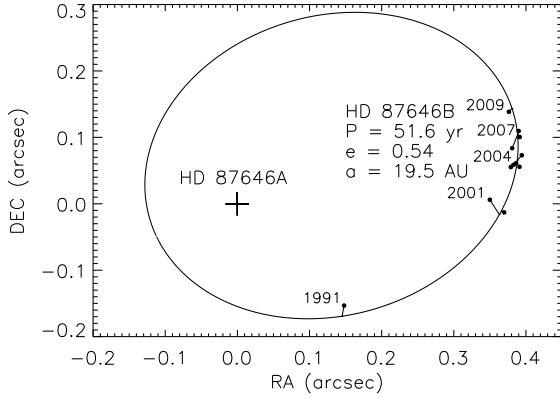


Fig. 8.— Orbital data for binary HD 87646. The plus symbol marks the location of the primary (HD 87646A), filled circles are measured position of HD 87646B from literature and this paper, and line segments are drawn from the ephemeris prediction to the observed location of the secondary in each case.

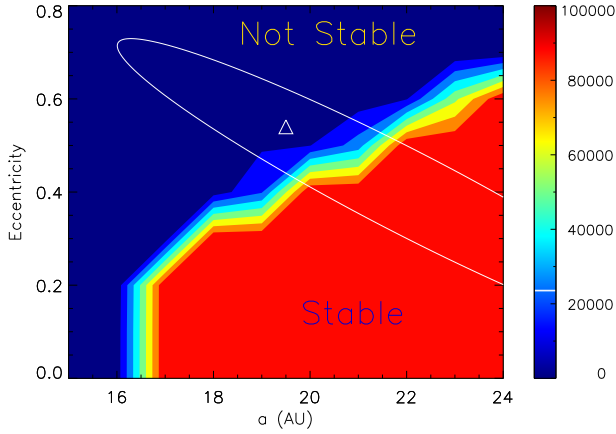


Fig. 9.— Dynamical simulation results for HD 87646. The contour lines show the time the system will remain stable according to our Mercury simulation. The unit of the color bar is years. A stable zone is found in the eccentricity-semimajor axis diagram, which shows that if the binary orbit has a large semi-major axis and low eccentricity, the system will remain stable. The white triangle symbol shows the best binary orbital fit from the current astrometry data with $\chi^2_{\text{red}} = 1$ after we rescale the error bars for astrometric data (see also Fig. 8). The white ellipse shows the distribution of binary orbital parameters from fitting the astrometric data fitting with $\max \chi^2_{\text{red}} = 2$. There is an overlap region between the distribution of binary orbital parameters and the dynamically stable region, which demonstrates the binary system has stable orbital solutions.

and hydrogen ($\sim 75M_{\text{Jup}}$, Chabrier et al. 2000) which are generally assumed to be the general mass boundaries between planet and brown dwarf and between brown dwarf and star, respectively. All these peculiarities raise a question: how could such a system be formed? Here we briefly discuss this intriguing issue.

The large masses of these two substellar objects suggest that they could be formed as stars with their binary hosts: a large molecular cloud collapsed and fragmented into four pieces; the larger two successfully became stars and formed the HD 87646 binary, and the other smaller ones failed to form stars and became the substellar objects in this system (Chabrier et al. 2014). This scenario might be relevant for the binary stars but seems problematic for the two substellar objects on orbits within ~ 1 AU because it is unclear whether fragmentation on such a small scale can occur (Kratter & Murray-Clay 2011).

Perhaps a more plausible explanation is that the two substellar objects were formed like giant planet in a protoplanetary disk around HD 87646A. As for giant planet formation, there are currently two main models: core accretion vs. disk instability (see the review by D’Angelo et al. 2010; Helled et al. 2014). Recently, many studies have examined the core accretion model’s ability to form planets in close binaries with separations of ~ 20 AU (see the review by Thebault & Haghighipour 2014, and the references therein). A commonly recognized issue is that the binary perturbations generally inhibit the growth of planetesimals in the disk (Thebault 2011). Even if their growth could proceed in certain favorable conditions (Xie & Zhou 2008, 2009), it would be significantly slowed, requiring a time scale of 10^6 yr or even longer (Xie et al. 2010). This result raises a problem for the formation of a gaseous giant planet, as it would not form a planetary core (via planetesimal growth) to accrete gas before the gas disk dissipation, which takes a timescale as short as 10^5 - 10^6 yr for such close binaries (Cieza et al. 2009; Kraus et al. 2012). Following the above logic, Xie, Zhou & Ge (2010) found that Jupiter-like planets are unlikely to form around Alpha Centauri B. As for the case of HD 87646, the formation of the two massive substellar objects via the core accretion model would be more problematic because it requires a more massive disk with mass larger than $68 M_{\text{Jup}}$. Such a massive disk is seldom observed in close binaries, which indicates that should such a massive disk exist, it would dissipate much faster than a normal lighter one.

Conversely, the disk instability model could circumvent most of the above barriers. First, disk instability usually requires very high disk mass, which is in line with the masses of the two detected substellar objects. Second, planet formation via disk instability requires a short timescale, which is also consistent with the short disk dissipation timescale observed in close binaries. In addition, the model of disk instability is recently advocated by Duchêne (2010), who argued that planet formation might be dominated by disk instability in close

binaries based on the fact that exoplanets within close binaries (separation < 100 AU) are significantly more massive than those within wide binaries or single stars. We could use the planet and brown dwarf mass to estimate the minimum surface density of the primordial disk, and test if such a disk is gravitationally unstable. We adopt the similarity solution of the evolving viscous disk (Hartmann et al. 1998) where the surface density follows R^{-1} from the star to the disk edge. Since the binary separation is 19 AU, the tidal truncation radius for the circumstellar disk around the primary star is ~ 6 AU (1/3 of the binary separation). Spreading the total mass of $12.4+57$ Jupiter mass to this 6 AU disk, the disk surface density at 6 AU is 2604 g/cm^2 . At 6 AU, the temperature is around 90 K with 1 solar luminosity. The sound speed is 0.56 km/s. Then the Toomre Q parameter with a 1.12 solar mass star is 1.5. At 1 AU, the temperature is around 220 K. The surface density is 15610 g/cm^2 . The sound speed is 0.87 km/s. The Toomre Q parameter is 5.7. Considering the primordial disk mass should be a lot more massive than the planet and brown dwarf mass, the disk is likely to be gravitationally unstable throughout the disk. This is consistent with gravitational instability leading to planet formation. Although several advantages exist for the disk instability model, we consider that such an explanation for the formation of the HD 87646 system should be taken with caution because whether disk instability can be triggered in the present of a close stellar companion remains an issue under debate (Nelson 2000; Mayer et al. 2005; Boss 2006).

Next we want to discuss how the giant planet, b, moved to its current position with a very low eccentricity. Although the Kozai-Lidov mechanism and subsequent tidal dissipation (Wu & Murray 2003; Fabrycky & Tremaine 2007) have been invoked often to explain the formation of hot Jupiters, it is unlikely that the brown dwarf, c, has helped to move b inward because such a process cannot help to form ‘warm’ Jupiters (Antonini et al. 2016). So we prefer a scenario in which b initially formed in the disk and then migrated inward in the disk to its current position, which explains why it has a near zero eccentricity. As for the brown dwarf, c, after it formed in the disk, scattering between c and other objects formed in the disk moved it to a higher eccentricity. During such a scattering process, lower mass objects tend to be ejected out and more massive objects are kicked inward with a higher eccentricity according to the simulation of Chatterjee et al. (2008). The stellar companion, B, cannot excite the eccentricity of c because Kozai oscillations will be destroyed by the presence of other massive sub-stellar objects in the system (in this case, the giant planet b) according to the studies of Wu & Murray (2003) and Fabrycky & Tremaine (2007). But the presence of the stellar companion, B, can help to enhance the scattering process between c and other objects formed in the protoplanetary disk around A (Marzari et al. 2005). Future astrometry observations, like those from Gaia (Perryman et al. 2001), can provide a better binary orbital solution and even possibly constrain the BD candidate’s orbit. These data

will help to study the dynamic structure of this complicated system and give more insight to its formation scenario.

Funding for the multi-object Doppler instrument was provided by the W.M. Keck Foundation. The pilot survey was funded by NSF with grant AST-0705139, NASA with grant NNX07AP14G and the University of Florida. Funding for SDSS-III has been provided by the Alfred P. Sloan Foundation, the Participating Institutions, the National Science Foundation, and the U.S. Department of Energy Office of Science. The SDSS-III web site is <http://www.sdss3.org/>. SDSS-III is managed by the Astrophysical Research Consortium for the Participating Institutions of the SDSS-III Collaboration including the University of Arizona, the Brazilian Participation Group, Brookhaven National Laboratory, Carnegie Mellon University, University of Florida, the French Participation Group, the German Participation Group, Harvard University, the Instituto de Astrofísica de Canarias, the Michigan State/Notre Dame/JINA Participation Group, Johns Hopkins University, Lawrence Berkeley National Laboratory, Max Planck Institute for Astrophysics, Max Planck Institute for Extraterrestrial Physics, New Mexico State University, New York University, Ohio State University, Pennsylvania State University, University of Portsmouth, Princeton University, the Spanish Participation Group, University of Tokyo, University of Utah, Vanderbilt University, University of Virginia, University of Washington, and Yale University. The research at Tennessee State University was made possible by NSF support through grant 1039522 of the Major Research Instrumentation Program. In addition, astronomy at Tennessee State University is supported by the state of Tennessee through its Centers of Excellence programs.

REFERENCES

- Alam, S., Albareti, F. D., Allende Prieto, C., et al. 2015, *ApJS*, 219, 12
- Alvarez M. et al., 1998, *A&A*, 340, 149
- Antonini, F., Hamers, A. S., & Lithwick, Y. 2016, arXiv:1604.01781
- D’Angelo, G., Durisen, R. H., & Lissauer, J. J. 2010, *Exoplanets*, 319
- Asplund M., 2005, *ARA&A*, 43, 481
- Balega I. I., Balega Y. Y., Gasanova L. T., Dyachenko V. V., Maksimov A. F., Malogolovets E. V., Rastegaev D. A., Shkhagosheva Z. U., 2013, *Astrophysical Bulletin*, 68, 53
- Barklem P. S., O’Mara B. J., 1998, *MNRAS*, 300, 863

- Boss A. P., 2006, *ApJ*, 643, 501
- Butler R. P., Marcy G. W., Fischer D. A., Vogt S. S., Tinney C. G., Jones H. R. A., Penny A. J., Apps K., 2004, in *IAU Symposium*, Vol. 202, *Planetary Systems in the Universe*, Penny A., ed., p. 3
- Chabrier G., Baraffe I., 2000, *ARA&A*, 38, 337
- Chabrier G., Johansen A., Janson M., Rafikov R., 2014, *Protostars and Planets VI*, 619
- Chambers, J. E. 1999, *MNRAS*, 304, 793
- Chatterjee, S., Ford, E. B., Matsumura, S., & Rasio, F. A. 2008, *ApJ*, 686, 580-602
- Cieza L. A. et al., 2009, *ApJ*, 696, L84
- Correia, A. C. M., Udry, S., Mayor, M., et al. 2008, *A&A*, 479, 271
- Duchêne G., 2010, *ApJ*, 709, L114
- Dumusque X. et al., 2012, *Nature*, 491, 207
- Eaton J. A., Williamson M. H., 2004, in *Society of Photo-Optical Instrumentation Engineers (SPIE) Conference Series*, Vol. 5496, *Advanced Software, Control, and Communication Systems for Astronomy*, Lewis H., Raffi G., eds., pp. 710–717
- Eaton J. A., Williamson M. H., 2007, *PASP*, 119, 886
- Eggenberger A., Udry S., Mazeh T., Segal Y., Mayor M., 2007, *A&A*, 466, 1179
- Eisenstein D. J. et al., 2011, *AJ*, 142, 72
- Erskine D. J., 2003, *PASP*, 115, 255
- Erskine D. J., Ge J., 2000, in *Astronomical Society of the Pacific Conference Series*, Vol. 195, *Imaging the Universe in Three Dimensions*, van Breugel W., Bland-Hawthorn J., eds., p. 501
- Fabrycky, D., & Tremaine, S. 2007, *ApJ*, 669, 1298
- Fekel F. C., Rajabi S., Muterspaugh M. W., Williamson M. H., 2013, *AJ*, 145, 111
- Feltzing S., Gustafsson B., 1998, *A&AS*, 129, 237
- Fischer D. A., Valenti J., 2005, *ApJ*, 622, 1102

- Fleming S. W. et al., 2010, *ApJ*, 718, 1186
- Ford E. B., 2006, *ApJ*, 642, 505
- Perryman, M. A. C., de Boer, K. S., Gilmore, G., et al. 2001, *A&A*, 369, 339
- Ge J., 2002, *ApJ*, 571, L165
- Ge J., Erskine D. J., Rushford M., 2002, *PASP*, 114, 1016
- Ge J., Mahadevan S., van Eyken J., Dewitt C., Shaklan S., 2003, in *Astronomical Society of the Pacific Conference Series*, Vol. 294, *Scientific Frontiers in Research on Extrasolar Planets*, Deming D., Seager S., eds., pp. 573–580
- Ge J. et al., 2006a, *ApJ*, 648, 683
- Ge J. et al., 2006b, in *Society of Photo-Optical Instrumentation Engineers (SPIE) Conference Series*, Vol. 6269, *Society of Photo-Optical Instrumentation Engineers (SPIE) Conference Series*, p. 2
- Ge J. et al., 2010, in *Society of Photo-Optical Instrumentation Engineers (SPIE) Conference Series*, Vol. 7735, *Society of Photo-Optical Instrumentation Engineers (SPIE) Conference Series*, p. 0
- Gonzalez A. H., Zaritsky D., Dalcanton J. J., Nelson A., 2001, *ApJS*, 137, 117
- Gould A. et al., 2014, *Science*, 345, 46
- Gregory P. C., 2005, *ApJ*, 631, 1198
- Gregory P. C., 2007, *MNRAS*, 381, 1607
- Gunn J. E. et al., 2006, *AJ*, 131, 2332
- Gustafsson B., Edvardsson B., Eriksson K., Jørgensen U. G., Nordlund Å., Plez B., 2008, *A&A*, 486, 951
- Han, E., Wang, S. X., Wright, J. T., et al. 2014, *PASP*, 126, 827
- Hartkopf W. I., Mason B. D., Worley C. E., 2001, *AJ*, 122, 3472
- Hartkopf, W. I., & Mason, B. D. 2009, *AJ*, 138, 813
- Hartmann, L., Calvet, N., Gullbring, E., & D’Alessio, P. 1998, *ApJ*, 495, 385

- Hatzes A. P., 2013, *ApJ*, 770, 133
- Helled, R., Bodenheimer, P., Podolak, M., et al. 2014, *Protostars and Planets VI*, 643
- Henry G. W., 1999, *PASP*, 111, 845
- Horch E. P., Falta D., Anderson L. M., DeSousa M. D., Minter C. M., Ahmed T., van Altena W. F., 2010, *AJ*, 139, 205
- Horch E. P., van Altena W. F., Cyr, Jr. W. M., Kinsman-Smith L., Srivastava A., Zhou J., 2008, *AJ*, 136, 312
- Howard, A. W., Johnson, J. A., Marcy, G. W., et al. 2010, *ApJ*, 721, 1467
- Howard A. W. et al., 2014, *ApJ*, 794, 51
- Howard A. W. et al., 2010, *Science*, 330, 653
- Kane S. R., von Braun K., 2008, *ApJ*, 689, 492
- Konacki M., 2005, *Nature*, 436, 230
- Kratter K. M., Murray-Clay R. A., 2011, *ApJ*, 740, 1
- Kraus A. L., Ireland M. J., Hillenbrand L. A., Martinache F., 2012, *ApJ*, 745, 19
- Kupka F., Piskunov N., Ryabchikova T. A., Stempels H. C., Weiss W. W., 1999, *A&AS*, 138, 119
- Lagrange A.-M., Beust H., Udry S., Chauvin G., Mayor M., 2006, *A&A*, 459, 955
- Lovis C. et al., 2006, *Nature*, 441, 305
- Ma B., et al., 2013, *AJ*, 145, 20
- Ma B., Ge J., 2014, *MNRAS*, 439, 2781
- Mahadevan S., van Eyken J., Ge J., DeWitt C., Fleming S. W., Cohen R., Crepp J., Vanden Heuvel A., 2008, *ApJ*, 678, 1505
- Marcy G. W., Butler R. P., 1992, *PASP*, 104, 270
- Mayer L., Wadsley J., Quinn T., Stadel J., 2005, *MNRAS*, 363, 641
- Mayor, M., & Queloz, D. 1995, *Nature*, 378, 355

- Marzari, F., Weidenschilling, S. J., Barbieri, M., & Granata, V. 2005, *ApJ*, 618, 502
- McArthur B. E. et al., 2004, *ApJ*, 614, L81
- Mugrauer M., Neuhäuser R., 2005, *MNRAS*, 361, L15
- Muterspaugh M. W. et al., 2010, *AJ*, 140, 1657
- Nakajima, T., Oppenheimer, B. R., Kulkarni, S. R., et al. 1995, *Nature*, 378, 463
- Nelson A. F., 2000, *ApJ*, 537, L65
- Nordstrom B. et al., 2008, *VizieR Online Data Catalog*, 5117, 0
- Ortiz, M., Reffert, S., Trifonov, T., et al. 2016, *arXiv:1608.00963*
- Oscoz, A., Rebolo, R., López, R., et al. 2008, *Proc. SPIE*, 7014, 701447
- Paegert, M., Stassun, K. G., De Lee, N., et al. 2015, *AJ*, 149, 186
- Perryman M. A. C., 1997, in *ESA Special Publication*, Vol. 402, *Hipparcos - Venice '97*,
Bonnet R. M., Høg E., Bernacca P. L., Emiliani L., Blaauw A., Turon C., Kovalevsky
J., Lindegren L., Hassan H., Bouffard M., Strim B., Heger D., Perryman M. A. C.,
Woltjer L., eds., pp. 1–4
- Plez B., Cohen J. G., 2005, *A&A*, 434, 1117
- Queloz D. et al., 2001, *A&A*, 379, 279
- Queloz D. et al., 2000, *A&A*, 354, 99
- Rajpaul V., Aigrain S., Roberts S., 2016, *MNRAS*, 456, L6
- Ramsey L. W. et al., 1998, in *Society of Photo-Optical Instrumentation Engineers (SPIE)*
Conference Series, Vol. 3352, *Advanced Technology Optical/IR Telescopes VI*, Stepp
L. M., ed., pp. 34–42
- Rebolo, R., Zapatero Osorio, M. R., & Martín, E. L. 1995, *Nature*, 377, 129
- Rivera E. J. et al., 2005, *ApJ*, 634, 625
- Robinson S. E., Strader J., Ammons S. M., Laughlin G., Fischer D., 2006, *ApJ*, 637, 1102
- Santos N. C. et al., 2004, *A&A*, 426, L19
- Santos N. C. et al., 2002, *A&A*, 392, 215

- Shetrone M. et al., 2007, *PASP*, 119, 556
- Spiegel D. S., Burrows A., Milsom J. A., 2011, *ApJ*, 727, 57
- Thebault P., 2011, *Celestial Mechanics and Dynamical Astronomy*, 111, 29
- Thebault P., Haghhighipour N., 2014, *ArXiv e-prints*
- Thomas, N., Ge, J., Grieves, N., Li, R., & Sithajan, S. 2016, *PASP*, 128, 045003
- Tody, D. 1993, *Astronomical Data Analysis Software and Systems II*, 52, 173
- Torres G., Andersen J., Giménez A., 2010, *A&A Rev.*, 18, 67
- Tull R. G., 1998, in *Society of Photo-Optical Instrumentation Engineers (SPIE) Conference Series*, Vol. 3355, *Optical Astronomical Instrumentation*, D’Odorico S., ed., pp. 387–398
- Udry S. et al., 2006, *A&A*, 447, 361
- van Eyken J. C., Ge J., Mahadevan S., 2010, *ApJS*, 189, 156
- van Eyken J. C., Ge J., Mahadevan S., DeWitt C., 2004, *ApJ*, 600, L79
- Wan X., Ge J., Guo P., Zhao B., Hariharan L., McDavitt D., 2006, in *Society of Photo-Optical Instrumentation Engineers (SPIE) Conference Series*, Vol. 6269, *Society of Photo-Optical Instrumentation Engineers (SPIE) Conference Series*, p. 2
- Wang J., Ge J., Wan X., De Lee N., Lee B., 2012a, *PASP*, 124, 1159
- Wang J., Ge J., Wan X., Lee B., De Lee N., 2012b, *PASP*, 124, 598
- Wolszczan, A., & Frail, D. A. 1992, *Nature*, 355, 145
- Wright J. T., 2005, *PASP*, 117, 657
- Wu, Y., & Murray, N. 2003, *ApJ*, 589, 605
- Xie J.-W., Zhou J.-L., 2008, *ApJ*, 686, 570
- Xie J.-W., Zhou J.-L., 2009, *ApJ*, 698, 2066
- Xie J.-W., Zhou J.-L., Ge J., 2010, *ApJ*, 708, 1566

Zhao B., Ge J., 2006, in Society of Photo-Optical Instrumentation Engineers (SPIE) Conference Series, Vol. 6269, Society of Photo-Optical Instrumentation Engineers (SPIE) Conference Series, p. 2

Zucker S., Mazeh T., Santos N. C., Udry S., Mayor M., 2003, A&A, 404, 775

Zucker S., Mazeh T., Santos N. C., Udry S., Mayor M., 2004, A&A, 426, 695